Technical University of Denmark

DTU

Gas Bearing Control for Safe Operation in Critical Speed Regions - Experimental Verification
Paper

Theisen, Lukas Roy Svane; Niemann, Hans Henrik; Galeazzi, Roberto; Santos, Ilmar

Link back to DTU Orbit

DTU Library
Technical Information Center of Denmark

Gas Bearing Control for Safe Operation in Critical Speed Regions - Experimental Verification

Gas Bearing Control for Safe Operation in Critical Speed Regions - Experimental Verification

Lukas R. S. Theisen[1]**, Hans H. Niemann**[1]**, Roberto Galeazzi**[1]**, Ilmar F. Santos**[2]

[1]Dept. of Electrical Engineering and [2]Dept. of Mechanical Engineering
Technical University of Denmark, DK 2800 Kgs. Lyngby, Denmark

E-mail: {lrst,hhn,rg}@elektro.dtu.dk, ifs@mek.dtu.dk

Abstract. Gas bearings are popular for their high speed capabilities, low friction and clean operation, but require low clearances and suffer from poor damping properties. The poor damping properties cause high disturbance amplification near the natural frequencies. These become critical when the rotation speed coincides with a natural frequency. In these regions, even low mass unbalances can cause rub and damage the machine. To prevent rubbing, the variation of the rotation speed of machines supported by gas bearings has to be carefully conducted during run-ups and run-downs, by acceleration and deceleration patterns and avoidance of operation near the critical speeds, which is a limiting factor during operation, specially during run-downs. An approach for reducing the vibrations is by feedback controlled lubrication. This paper addresses the challenge of reducing vibrations in rotating machines supported by gas bearings to extend their operating range. Using $\mathcal{H}_\infty$-design methods, active lubrication techniques are proposed to enhance the damping, which in turn reduces the vibrations to a desired safe level. The control design is validated experimentally on a laboratory test rig, and shown to allow safe shaft rotation speeds up to, in and above the two first critical speeds, which significantly extends the operating range.

1. Introduction

Gas bearings offer clean operation with low friction, but suffer from poor damping properties and require low clearances. Rotating machines supported by gas bearings are therefore very sensitive towards mass unbalance and disturbances. The natural frequencies especially become critical as they coincide with the rotation speed, where the mass unbalance response grows until the shaft rubs the bearing surface. Operation near the critical speeds is therefore avoided, which limits the usability of the machines. An ad-hoc approach to reduce vibrations when crossing the critical speeds, is to quickly accelerate rotation shaft across the critical speed before the full vibration amplitude is obtained. Such an approach however results in the "cat in the tree"-problem - it may be easy to get up, but difficult to get safely down again. Due to the low viscosity there are almost no friction losses, which in turn results in a slow deceleration of the shaft. This gives enough time for the undesired vibrations to build up.

For a given fixed machine design, the shaft vibrations can be reduced in two ways. Proper balancing of the shaft can drastically reduce mass unbalance, but not eliminate it. Further this obviously does not diminish sensitivity to external disturbances. Active lubrication techniques through feedback control represent a valid alternative approach, which can handle both mass

unbalance and external disturbances. Feedback control has been widely applied to active magnetic bearing (AMB)-systems. Many authors have proposed various control designs, e.g. linear parameter-varying (LPV)-controllers to eliminate the mass unbalance response by placing closed-loop zeros in the sensitivity function at the shaft rotation speed. e.g. in [1, 3, 11]. Such controllers completely eliminate the mass unbalance at the cost of a high control effort. The use of phase shift filters has also been proposed in literature [12]. These mentioned approaches only reject disturbances at the rotational frequency.

Previous papers [5,9,10] on control of gas bearings have treated design of classical controllers, but none of these had sufficient robustness, and therefore were not able to reduce vibrations enough to allow a safe crossing of the critical speed. In [8] we proposed an $\mathcal{H}_\infty$ and an LPV controller to enhance the damping of the gas bearing. The controllers were found able to both reject the external disturbances and reduce the vibration amplitude within the considered operating range.

In continuation of that work, this paper explores further the capabilities of such designs. The same $\mathcal{H}_\infty$ setup is used to obtain a damping enhancing controller, and the vibration reduction capabilities are investigated to extend the region of operation. The available model relies on open loop identification, which poses a challenge, since open loop operation is not possible in these regions. A controller is therefore required, which should again be validated from a model of the system at that particular operating condition. Instead, an alternative must be sought. Our approach therefore relies on designing a controller from the LPV model inside the identified region, and investigating the controller performance outside the identified region. The upper limits for safe rotation are investigated both for closed loop experiments and open loop experiments.

The paper is structured as follows. Section 2 contains an overview of the test rig utilised for experimental validation and some highlights of the model of the gas bearing. The design of the $\mathcal{H}_\infty$ controller is detailed in Section 3, and the available LPV model is used in extrapolation to provide an expectation of the controller performance for higher rotation speeds. This performance is investigated experimentally in Section 4. Last, some conclusions are drawn and future aspects are discussed in Section 5.

Notation

The paper uses upper case bold letters for matrices $\mathbf{A}$, lower case bold letters for vectors $\mathbf{a}$, the Laplace variable is denoted s. Continuous time signals are addressed $a(t)$. Signals in the Laplace domain are addressed $a(s)$, and sampled signals at time instants kT_s are denoted $a(kT_s)$. State-space dynamics is formulated in shorthand as $\mathbf{G} = \left[\begin{array}{c|c}\mathbf{A} & \mathbf{B} \\ \hline \mathbf{C} & \mathbf{D}\end{array}\right]$, which defines the state-space relation $\left[\begin{array}{c}\dot{\mathbf{x}} \\ \mathbf{y}\end{array}\right] = \mathbf{G}\left[\begin{array}{c}\mathbf{x} \\ \mathbf{u}\end{array}\right] = \left[\begin{array}{c|c}\mathbf{A} & \mathbf{B} \\ \hline \mathbf{C} & \mathbf{D}\end{array}\right]\left[\begin{array}{c}\mathbf{x} \\ \mathbf{u}\end{array}\right]$. The identity matrix of size n is denoted $\mathbf{I}_n$. Shaft rotation speed units are given in Hz, though the common in rotordynamics is revolutions per minute: $(1\ Hz = 60\ rpm)$.

2. Controllable Gas Bearing
2.1. Test Rig
The experimental controllable gas bearing setup at hand is shown in Fig. 1. It consists of a turbine (1) driving a flexible shaft (2) supported by both a ball bearing (3) and the controllable gas bearing (4), in which pressurised air is injected through four piezoactuated injectors numbered as shown. The injection pressure is constant $P_{\text{inj}} = 0.3\ MPa$, which is measured before splitting up to the four piezoactuators. The pressure is not controlled, but the variations are negligible. A disc (5) is mounted in one end to pre-load the journal. The horizontal and vertical disc movement $\mathbf{p} \triangleq [p_x, p_y]^{\mathrm{T}}$ is measured at the disc location using eddy current sensors (6) in the coordinate frame specified in the figure. For zero input and when the
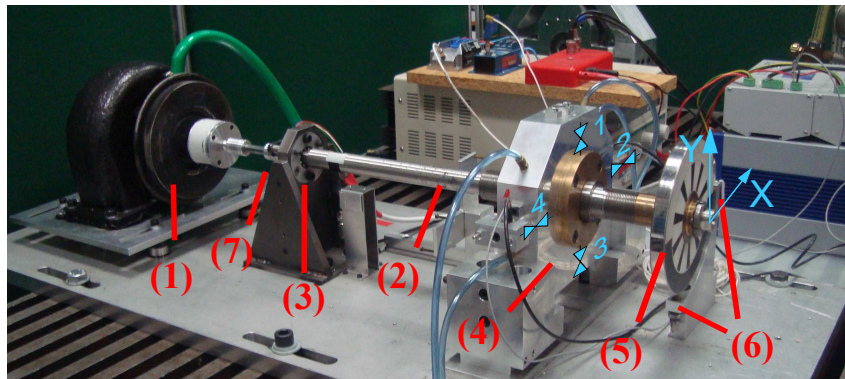
Figure 1. The experimental controllable gas bearing setup. A turbine (1) drives a flexible shaft (2), which is supported by both a ball bearing (3) and the controllable gas bearing (4) with four piezoactuated injectors. A disc (5) is mounted in one end to pre-load the journal and displacement sensors (6) measure the lateral movement of the disc in the shown reference frame. A quadrature encoder (7) measures the angular position.

rotor is at stand still, the position is $\mathbf{p} = \mathbf{0}$. The angular position of the rotor ϕ is measured by an optical quadrature encoder (7), from which the rotation speed Ω is calculated. The injectors are controlled in a pairwise differential mode. Thereby one piezoactuator reference r_x is sent to control the position of the horizontal injectors, and one reference r_y is sent to control the vertical ones. These references are in intervals $[-5, 5]$ V, which corresponds to full-span motion of the piezoactuator positions in the interval $[0, 45]$ μm. The nominal clearance of the gas bearing is 25 μm. Given the right conditions of sufficient injection pressure and sufficiently low rotational speed, the gas film generates restoring forces and thereby keeps the rotor levitating about a stable equilibrium. All measurements are sampled with period $T_s = 0.2$ ms. A detailed description of the setup is available in [4].

For equipment safety, the vibrations must be within a safety region, in this case chosen as a circle:

$$x_s = r \cdot cos(\theta) - x_0, \quad y_s = r \cdot sin(\theta) - y_0, \quad \theta \in [0, 2\pi[\ rad \tag{1}$$

Manual tests were performed to assess safe limits of the circle parameters, and the following were found sufficiently conservative: radius $r = 20\mu m$, and centre $x_0 = 10\mu m$, $y_0 = -3\mu m$. These limits are deliberately chosen to be conservative for equipment safety.

2.2. Gas Bearing Model
The gas bearing test rig is modelled using the linear parameter-varying (LPV)-identification approach from [10], where local LTI-models are identified from data collected in a grid of injection pressures and shaft rotation speeds. For the present work, the injection pressure is kept constant, and the model is then only function of the rotation speed. The identification grid contained six uniformly spaced shaft rotation speeds in the interval $\Omega \in [0, 92]$ Hz. The model can be decomposed to a cascade coupling of the actuator dynamics $\mathbf{G}_{act}$, time delays $\mathbf{G}_{\tau}$ and the rotor-bearing dynamics $\mathbf{G}_{rb}$:

$$\mathbf{G}(t, \Omega) = \mathbf{G}_{rb}(t, \Omega)\mathbf{G}_{\tau}(t, \Omega)\mathbf{G}_{act}(t) \tag{2}$$

The actuator dynamics are independent of the scheduling parameter and have the following diagonal second order form with two real poles and a gain:

$$\mathbf{G}_{act}(s) = \begin{bmatrix} G_{a,x}(s) & 0 \\ 0 & G_{a,y}(s) \end{bmatrix}, \qquad G_{a,j}(s) = \frac{\kappa_{a,j}}{\left(\frac{1}{p_{1,j}}s+1\right)\left(\frac{1}{p_{2,j}}s+1\right)}, \quad j \in \{x,y\} \qquad (3)$$

The rotor-bearing dynamics is modelled as the interconnection of a parameter-varying delay and a second order parameter-varying mass-spring-damper system. The latter has a state-space realisation:

$$\mathbf{G}_{rb} = \left[\begin{array}{cc|c} \mathbf{0}_2 & \mathbf{I}_2 & \mathbf{0}_2 \\ \mathcal{K}(\Omega) & \mathcal{D}(\Omega) & \mathcal{B}(\Omega) \\ \hline \mathbf{I}_2 & \mathbf{0}_2 & \mathbf{0}_2 \end{array} \right] \qquad (4)$$

in which the parameter-varying matrices $\{\mathcal{K}, \mathcal{D}, \mathcal{B}\}$ are second order polynomials in the rotation speed Ω. The delays are second order polynomials in rotation speed, and finite models are obtained by a first order Padé approximation:

$$\mathbf{G}_{\boldsymbol{\tau}}(t,\Omega) = \begin{bmatrix} G_{\tau_x(\Omega)}(t) & 0 \\ 0 & G_{\tau_y(\Omega)}(t) \end{bmatrix}, \qquad G_{\tau_j(\Omega)}(t) = \left[\begin{array}{c|c} -2/\tau_j(\Omega) & 1 \\ \hline 4/\tau_j(\Omega) & -1 \end{array} \right], \quad j \in \{x,y\} \qquad (5)$$

The natural frequencies of the LPV model change with rotation speed but are approximately $\omega_1 = 105\ Hz$ and $\omega_2 = 115\ Hz$. It is desired to extend the region of safe operation, which implies increasing the rotation speed to values outside the identification region. The actuator dynamics contains only real poles acting at frequencies higher than $400Hz$. Since actuation in this range of frequencies is not desired, the actuator dynamics is approximated by a static gain. The gas bearing model is then of order $n = 6$.

The nominal model is chosen as the LPV model evaluated at $91\ Hz$.

$$\mathbf{G} = \mathbf{G}(t,\Omega)\Big|_{\Omega = 91\ Hz} \qquad (6)$$

The mass unbalance is not included in the model, but acts as a force on the shaft given by:

$$\mathbf{f}_u = m_u e_u \Omega^2 \begin{bmatrix} \sin(\Omega t + \varphi) \\ \sin(\Omega t - \pi/2 + \varphi) \end{bmatrix} \qquad (7)$$

in which Ω is the shaft rotation speed, m_u is the unknown unbalance mass, and e_u is the unknown distance between the mass unbalance and the geometrical shaft centre, and φ is the phase of the disturbance. This can be modelled as an input disturbance in the gas bearing. The force from mass unbalance therefore grows by Ω^2 as the rotation speed increases, and the response is greatly amplified near the resonance frequencies. At this point, the mass unbalance remains largely unknown except for its frequency, which suffices for control design.

3. $\mathcal{H}_\infty$ Control Design

This section details the damping enhancing $\mathcal{H}_\infty$ control design from [8] to allow the safe crossing of the first two critical speeds by reducing the vibrations to be within the desired safety region from Eq. (1). These requirements are not easily included directly in the $\mathcal{H}_\infty$ setup especially since the mass unbalance is largely unknown. Instead, the controller $\mathbf{K}$ should enhance the damping and thereby reduce the gain magnitude at the resonance frequencies without wearing the actuator out. These disturbance and noise rejection requirements are formulated using the mixed sensitivity setup [7], which seeks to minimise:

$$\mathbf{K}^* = \arg\min_{\mathbf{K}} \|\mathbf{N}\|_\infty, \quad \mathbf{N} = \begin{bmatrix} \mathbf{W}_p \mathbf{S} \\ \mathbf{W}_u \mathbf{K} \mathbf{S} \end{bmatrix}, \qquad (8)$$
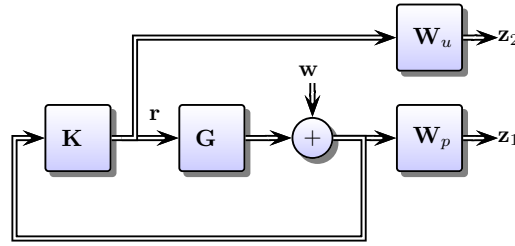
Figure 2. The augmented plant with controller for LPV controller design with performance weights $\mathbf{W}_p$ and controller sensitivity weight $\mathbf{W}_u$.

where the closed loop sensitivity functions for a given $\Omega = \bar{\Omega}$ are :

$$\mathbf{S}(s,\bar{\Omega}) \triangleq (\mathbf{I} + \mathbf{GK})^{-1} \tag{9}$$

and $\mathbf{KS}$ represents the control sensitivity. They are shaped by the weight functions $\mathbf{W}_p$ and $\mathbf{W}_u$. The external output disturbance $\mathbf{w}$ and external outputs $\mathbf{z} = [\mathbf{z}_1^{\mathrm{T}}, \mathbf{z}_2^{\mathrm{T}}]^{\mathrm{T}}$ are included into the system to obtain the augmented plant as shown in Fig. 2. The controller then satisfies $\|\mathbf{N}\|_\infty < \gamma$.

To enhance damping, the controller should have high performance in the frequency range around the under-damped eigenfrequencies of the rotor-bearing ω_x and ω_y. The performance filter is therefore chosen to contain inverse notch like filters:

$$\mathbf{W}_p(s) = \mathrm{diag}\left(w_{px}(s), w_{py}(s)\right) \tag{10}$$

in which w_{px} and w_{py} both have the form:

$$w_{px}(s) = \frac{s^2 + 2\zeta_1\omega_x s + \omega_x^2 k_0}{s^2 + 2\zeta_2\omega_x s + \omega_x^2}, \quad w_{py}(s) = \frac{s^2 + 2\zeta_1\omega_y s + \omega_y^2 k_0}{s^2 + 2\zeta_2\omega_y s + \omega_y^2} \tag{11}$$

The natural frequencies ω_x, ω_y are chosen as the under-damped natural frequencies of the gas bearing to obtain a high weight around these. The weight at the resonance frequencies is set to 19 dB, which is obtained by the damping factors $\zeta_1 = 0.3$ and $\zeta_2 = 0.05$. The low sensitivity around the natural frequencies must come at the cost of increased sensitivity in another frequency range due to Bode's sensitivity integral [2]. It was argued in [9] to place this sensitivity increase in the low frequency range, where an amplification of mass unbalance and disturbances is acceptable. The constant $k_0 = 1/3$ determines the low frequency weight, and the sensitivity at low frequency is guaranteed to be less than γk_0. The control signal sensitivity weight $\mathbf{W}_u$ is chosen to penalise control action at high frequency. This is achieved with the high-pass filter from [7, Sec. 2, Eq. (2.72)]:

$$\mathbf{W}_u(s) = \mathbf{I} w_u(s), \quad w_u(s) = \frac{s/M_b + \omega_b}{s + \omega_b A_b}, \tag{12}$$

where the low frequency gain is $1/A_b$, $A_b = 10$; the high frequency gain is $1/M_b = 15$, and the approximate crossover frequency is $\omega_b = 2000\pi$ rad/s. The weights are shown in Fig. 3. Since $|\mathbf{S}| > 1$ for low frequencies, the controller amplifies mass unbalance for low rotation speeds, which is affordable, whereas at high rotation speeds, the vibrations are attenuated. A 12-th order $\mathcal{H}_\infty$ controller is synthesised with $\gamma = 1.15$ and the performance shown in Fig. 4. At low
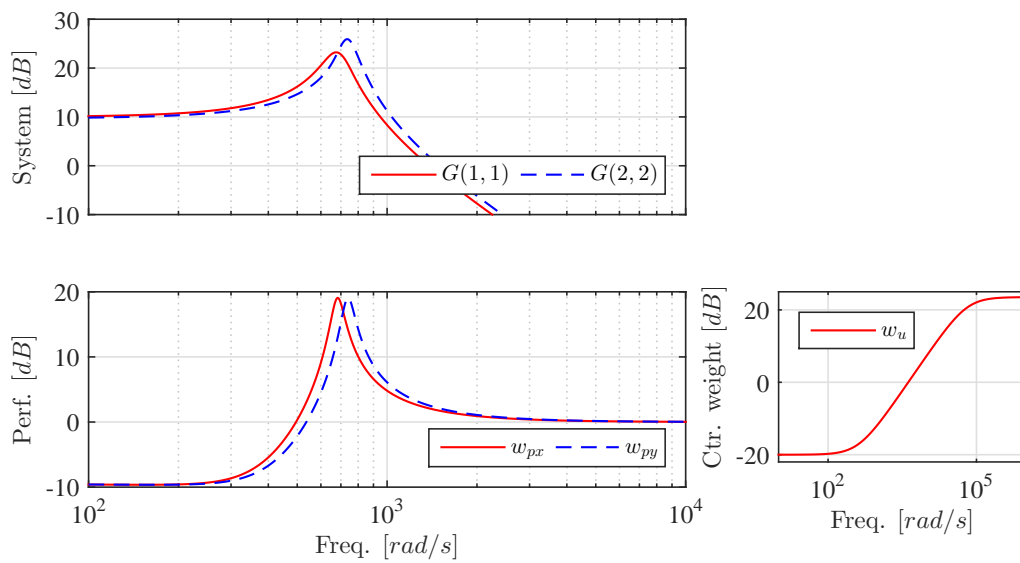
Figure 3. System gain, performance weights $w_{px}(s)$, $w_{py}(s)$ as defined in Eq. (11) and controller sensitivity weight $w_u(s)$ as defined in Eq. (12). The two left plots share the frequency axis to show the performance weight peaks coincide with the natural frequencies.
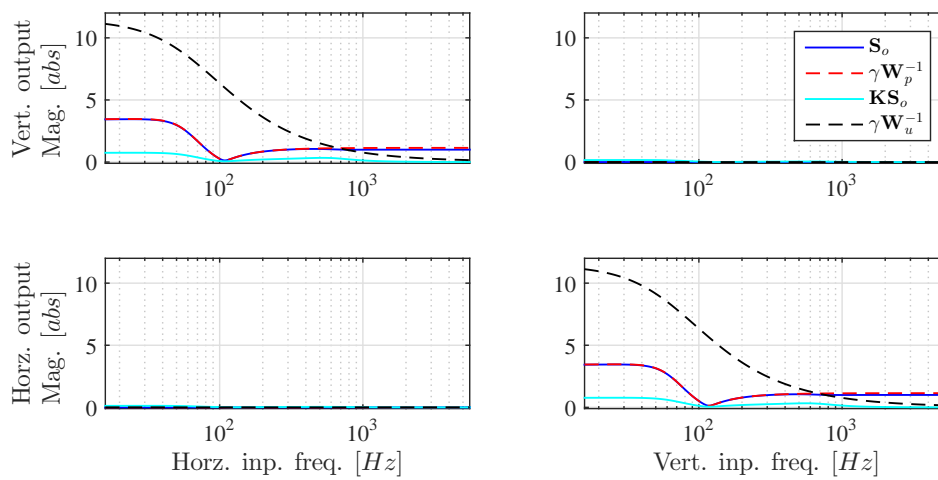

Figure 4. Resulting sensitivity functions $\mathbf{S}$ and $\mathbf{KS}$ and corresponding inverse scaled weights $\gamma\mathbf{W}_p^{-1}$ and $\gamma\mathbf{W}_u^{-1}$. At low frequency, the performance closely follows the performance weight.

frequencies up to above the first two critical speeds, the performance is limited by **S** as desired, whereas at high frequency, **KS** becomes limiting.

To allow implementation on the dSpace system, the controller is converted to discrete time using Tustin transformation and sampling frequency $f_s = 5\ kHz$.

3.1. Closed-Loop Performance Assessment Based on Extrapolated LPV Model
Since no gas bearing model is available for rotational speeds higher than 92 Hz, the performance of the controller is attempted to be assessed by means of model extrapolation from the identified LPV model. The performance assessment is strongly affected by the extrapolation, therefore the obtained results must be carefully interpreted. The LPV model Eq. (6) is extrapolated for various rotation speeds, and used to calculate the loop sensitivities using Eq. (9). The results are shown in Fig. 5. In open loop, the input disturbances are greatly amplified near the resonances, whereas the closed loop disturbance functions **SG** show a significant reduction in disturbance gain as desired. The controller has low sensitivity near the resonance frequencies, and obtains $|\mathbf{S}| < 1$ in an interval above the resonance frequencies. This indicates that the controller reduces the mass unbalance both before and after the critical speeds are crossed. Investigations also show, that the control effort **KS** is sufficiently low. The performance analysis based on the extrapolated models suggests that the designed controller may succeed in increasing the system damping at and about the critical frequencies. The validity of these predictions needs to be verified experimentally, and this is shown in the following section.

4. Experimental Results
The results of the previous section should be investigated experimentally, both the open loop and the closed loop.

This is done by applying the controller at low speed, and then slowly accelerating the shaft while monitoring the vibration amplitude. A standard runout filter is applied to remove artefacts from the measurements from mechanical imperfections in the disk using the procedure described in [10]. At standstill, the rotor equilibrium position is below the geometric bearing centre [6]. The given shaft positions **p** correspond to deviations from the equilibrium position. Two different experiment types where performed to assess the upper limit of safe rotation speed: an open loop and a closed loop. To avoid rotor-bearing rubbing during experiments, the shaft rotation speed is increased slowly until the vibrations exceed the safety region. The vibrations of the open loop experiment are shown in Fig. 6. At $\Omega = 94.8\ Hz$, the vibrations exceed the safety region, and the rotor reaches a speed of $\Omega = 97.5\ Hz$ before the experiment is stopped. The critical speeds can therefore not be crossed safely in open loop. During the closed loop experiment, the shaft is again accelerated slowly allow the vibrations to build up during the operation. A bias is applied to the control signal to allow a shift of the vibrations' centre. According to the model, the critical speeds are expected to be near $105\ Hz$ and $115\ Hz$. It is evident, that the shape of the vibrations changes near these speeds. These speeds are crossed very slowly to allow the vibrations to build up and validate, the critical speeds pose no challenge in closed loop. The rotation speed can therefore be increased even further. During the experiment, the rotor reaches a speed of $\Omega = 153\ Hz$ where the control signals approaches the level of saturation. Such saturation in best case deteriorates the performance, but potentially destabilises the system. It is therefore decided to stop the experiment.

The vibrations are often investigated in rotor-dynamics as function of the rotation speed in a waterfall diagram. This is obtained as the FFT of smaller sections of the data. Such a diagram is shown for the vertical shaft direction in Fig. 7 for both the open loop and the closed loop case. The synchronous vibrations for $\Omega > 50Hz$ are significantly reduced in the closed loop case, and the critical speeds can therefore be crossed safely. It may be argued, that the approach of
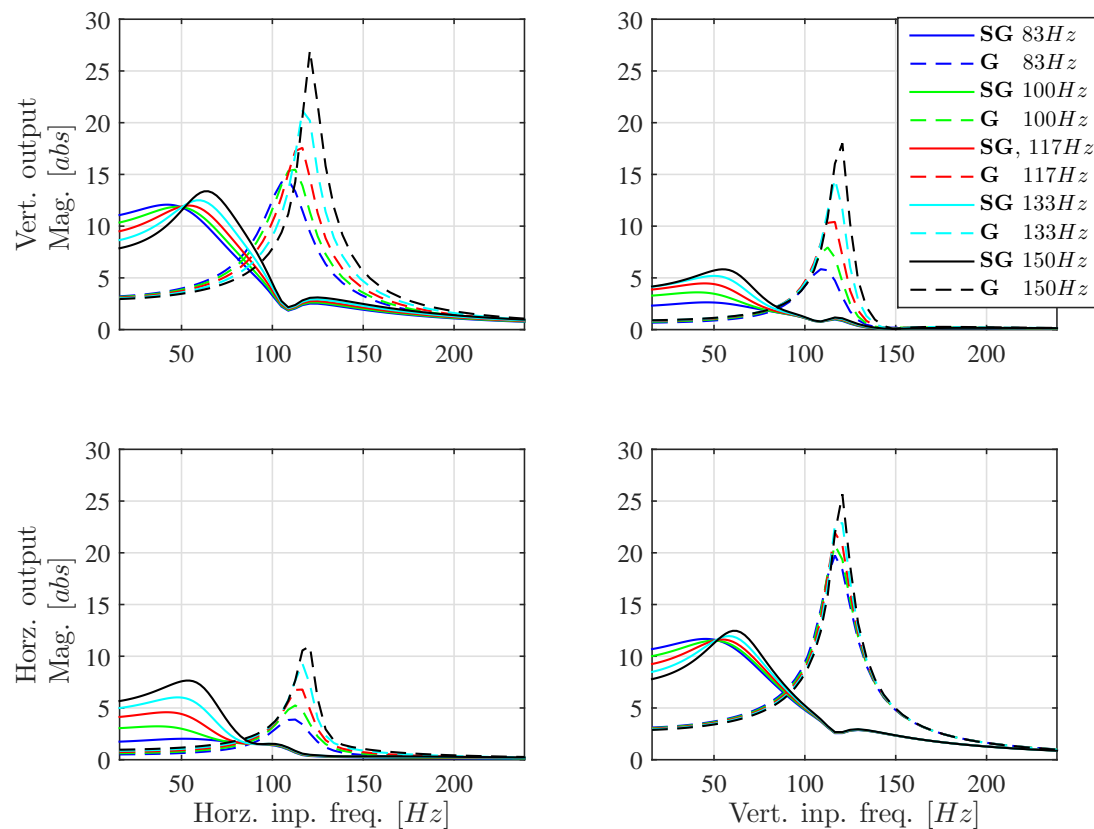
Figure 5. Evaluation of open and closed loop input disturbance responses (**G** , **SG**) for different rotation speeds extrapolated with the LPV model. The model shows, that the controller reduce the peak gain significantly.

applying an input bias should also have been used in the open loop experiment, but the vibration amplitude would still quickly have grown exceeded the allowed vibration level.

A later experiment was performed, where the rotor speed was increased even further up to $\Omega = 161.4 \ Hz$, and the vibrations were within the desired level. This corresponds to an increase in operating range of approximately 70%.

5. Conclusions and Future Aspects
This paper investigated control designs to reduce the vibrations in rotating machinery supported by gas bearings. A controller was designed using the developed LPV model, and experimental results demonstrated the feasibility of using the controller to extend the operation range. The controller allowed rotation speeds up to, in and above the first two critical speeds, which extended the operation range by 70%. Future experiments will investigate the performance as the rotation speed is increased even further. In this region, sub-synchronous whirl dominates the response, and it is of interest to use controllers to postpone the onset of the whirl [4].

References
[1] H. M. N. K. Balini, J. Witte, and C. W. Scherer. Synthesis and implementation of gain-scheduling and lpv controllers for an amb system. *Automatica*, 48(3):521–527, 2012.
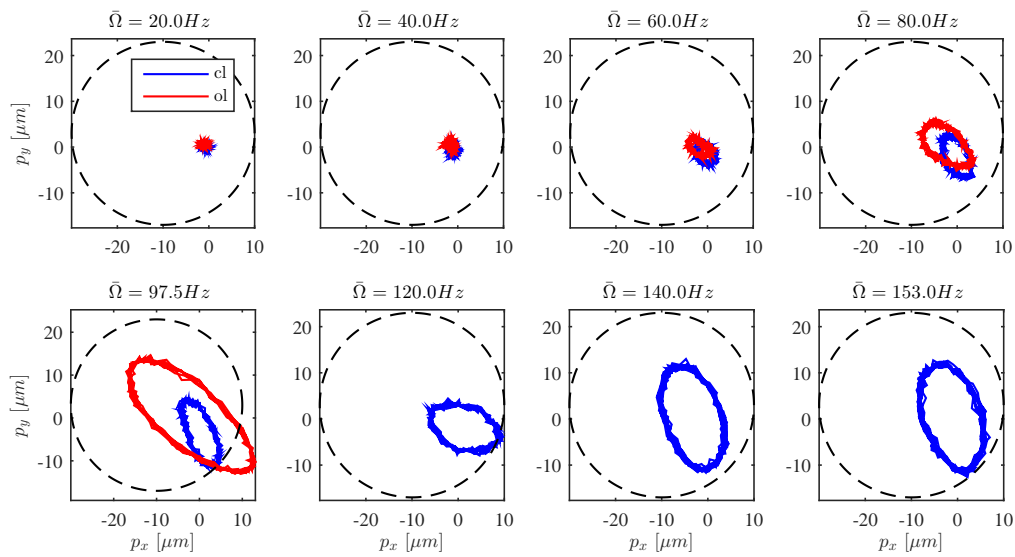
Figure 6. Experimental measurements for various shaft rotation speeds. In open loop (ol), the vibrations exceed the limit of safe operation at $\Omega = 94.8 \ Hz$. In closed loop (cl), the control reduces the vibrations and significantly increases this limit.
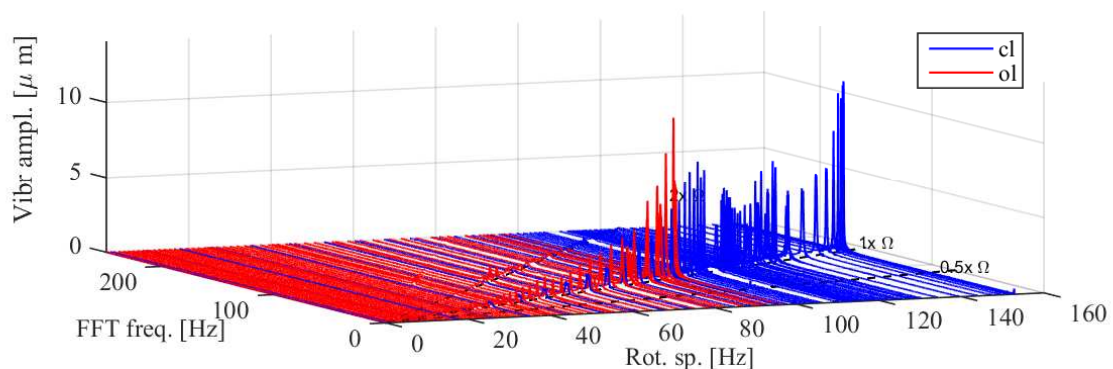

Figure 7. Waterfall diagram for vertical shaft direction to investigate the frequency content of the vibrations. In open loop (ol) the synchronous vibrations grow fast as the critical speed is approached. In closed loop (cl), the vibrations are sufficiently attenuated to allow faster rotation speeds.

[2] J. S. Freudenberg and D. P. Looze. Right half plane poles and zeros and design tradeoffs in feedback systems. *IEEE Transactions on Automatic Control*, 30(6):555–565, 1985.

[3] S. Mason, P. Tsiotras, and P. Allaire. Linear parameter varying controllers for flexible rotors supported on magnetic bearings. 2009.

[4] S. Morosi and I. F. Santos. *From Hybrid to Actively-Controlled Gas Lubricated Bearings Theory and Experiment*. PhD thesis, Technical University of Denmark, 2011.

[5] S. Morosi and I. F. Santos. Experimental investigations of active air bearings. In *Proceedings of ASME Turbo Expo 2012*, volume 7, pages 901–910. American Society of Mechanical Engineers, 2012.

[6] F. G. Pierart and Ilmar F. Santos. Steady state characteristics of an adjustable hybrid gas bearing - computational fluid dynamics, modified reynolds equation and experimental validation. *Proc. Inst. Mech. Eng. Part J.-j. Eng. Tribol*, 229(7):807–822, 2015.

[7] S. Skogestad and I. Postlethwaite. *Multivariable Feedback Control: Analysis and Design*. John Wiley & Sons, 2005.

[8] L. R. S. Theisen, H. H. Niemann, R. Galeazzi, and I. F. Santos. Enhancing damping of gas bearings: Comparison of $\mathcal{H}_\infty$ and lpv-control, theory & experiment. *Submitted to IEEE Trans. on Control Systems Technology*, 2015.

[9] L. R. S. Theisen, H. H. Niemann, I. F. Santos, and R. Galeazzi. Experimental investigations of decentralised control design for the stabilisation of rotor-gas bearings. In *Proceedings of the XVII International Symposium on Dynamic Problems of Mechanics*, 2015. In press.

[10] L. R. S. Theisen, H. H. Niemann, I. F. Santos, R. Galeazzi, and M. Blanke. Modelling and identification for control of gas bearings. *Mechanical Systems and Signal Processing*, pages –, 2015.

[11] J. Witte, H.M.N.K. Balini, and C.W. Scherer. Robust and LPV control of an AMB system. *American Control Conference (ACC), 2010*, pages 2194–2199, 2010.

[12] S. Zheng, B. Han, Y. Wang, and J. Zhou. Optimization of damping compensation for a flexible rotor system with active magnetic bearing considering gyroscopic effect. *Ieee-asme Transactions on Mechatronics*, 19(4):1130–1137, 2014.